Available online at www.sciencedirect.com
ScienceDirect
Journal of Colloid and Interface Science 309 (2007) 518–523
JOURNAL OF Colloid and Interface Science
www.elsevier.com/locate/jcis

One-step controlled synthesis of anisotropic gold nanostructures with aniline as the reductant in aqueous solution

Zhirui Guo [a,b], Yu Zhang [a,b], Lan Huang [a], Meng Wang [a,b], Jing Wang [a], Jianfei Sun [a,b], Lina Xu [a], Ning Gu [a,b,*]

[a] *State Key Laboratory of Bioelectronics, Southeast University, Nanjing 210096, China*
[b] *Jiangsu Laboratory for Biomaterials and Devices, Southeast University, Nanjing 210096, China*

Received 3 July 2006; accepted 31 December 2006
Available online 14 February 2007

Abstract

We report a general and versatile method for controlled synthesis of anisotropic gold nanostructures through the reduction of $HAuCl_4$ by aniline in aqueous solution, without the need for an additional stabilizer or capping agent. In this approach, the reduction kinetics of $AuCl_4^-$ can be altered by simply adjusting the initial pH and temperature, inducing the formation of a wide variety of anisotropic nanostructures such as dispersed or multilayered plates, wires with networked or paramecium-like structures, and ginger-shaped particles. AFM, TEM, XRD, EDX, FTIR, and UV–vis–NIR measurements were used to characterize the resulting gold nanostructures. Investigation reveals that in situ formed polyaniline serves effectively as a capping agent to direct the shape of gold nanostructures during the slow growth process. These as-synthesized gold nanostructures exhibit strongly shape-dependent optical properties. This facile approach may be extended to the synthesis of some other anisotropic metal nanostructures such as platinum or palladium.

Keywords: Gold; Anisotropic shape; Nanostructure; Aniline; pH

1. Introduction

Metal nanostructures have received significant attention due to their unique electronic, magnetic, optical, biological, and catalytic properties [1,2]. Currently, there is increasing interest in developing methods for generating metal nanostructures with specific shapes, because their physical and chemical properties are strongly shape-dependent. For example, the ultraviolet–visible–near infrared (UV–vis–NIR) absorption spectrum of gold nanorods shows two absorption peaks arising from the transverse and longitudinal surface plasmon resonances (SPR), whereas that of spherical gold nanoparticles displays a single SPR peak around 520 nm [3]. It has also been confirmed that platinum nanocubes with a surface composed mainly of {100} facets have higher catalytic selectivity than spherical platinum nanoparticles composed of {111} and {100} facets during the methane reduction of nitrogen oxide [4]. Among the strategies for shape-controlled synthesis of metal nanostructures, solution-phase synthesis is promising for the wide applicability, potential high yields, and relatively low cost it offers. To date, gold nanostructures with diverse shapes, such as plates [5–9], wires [10–12], ribbons [13], multipods [14,15], dendrites [16], and tadpoles [17], have been synthesized using this strategy. However, most of the above approaches could yield only one or two different shapes (spheres included) through changing the reaction parameters and generally required the introduction of additional stabilizers. Hence, novel versatile but simple approaches to producing metal nanostructures with specific shapes are still highly desirable.

Recently, the synthesis of spherical gold nanoparticles employing aniline as both reductant and subsequent stabilizer, in the form of polyaniline, has been reported [18–20]. However, anisotropic gold nanostructures obtained using aniline as the reductant in aqueous solution have rarely been reported to date. Here, we demonstrate that the kinetics of reduction of $AuCl_4^-$

* Corresponding author.
E-mail address: guning@seu.edu.cn (N. Gu).

0021-9797/$ – see front matter
doi:10.1016/j.jcis.2006.12.070

by aniline can be greatly altered by varying the initial pH (denoted by pH_0) value and reaction temperature and, thus, inducing the formation of gold nanostructures with different shapes, including dispersed or multilayered plates, curly wires with networked or paramecium-like structures, and ginger-shaped particles, without the need of additional stabilizers or capping agents. The formed polyaniline in situ could also serve effectively as a capping agent to direct the shape of gold nanostructures during the slow growth process. The corresponding UV–vis–NIR absorption spectra of these gold nanostructures display strongly shape-dependent SPR absorption characteristics.

2. Experimental section

2.1. Chemicals

All chemicals were analytically pure and purchased from Shanghai Chemical Reagent Co. Ltd. (China). Aniline was distilled twice under reduced pressure in the presence of zinc powder and stored in a brown bottle. $HAuCl_4{\cdot}4H_2O$, HCl (37% w/w), NaOH, anhydrous ethanol, and *N*-methyl-2-pyrrolidone (NMP) were used as received without further purification. Millipore-quality water was used for all solution preparations. The pH of the $HAuCl_4$ solutions was adjusted prior to reaction by addition of aqueous 1 M HCl or 1 M NaOH.

2.2. Synthesis of gold nanostructures with different shapes

In a typical synthesis, 50 ml of aqueous 0.72 mM $HAuCl_4$ with a certain pH_0 was added to a flask equipped with a condenser and heated to 80 °C, after which aqueous 0.1 M aniline was rapidly added to yield a 3:1 molar ratio of aniline to gold under vigorous stirring. After 2 h the gold product was isolated by centrifugation and washed several times with ethanol followed by water. The product was then redispersed in water for further characterization. Synthesis of gold nanostructures at 60 °C and room temperature followed the same procedure, except that at room temperature the reaction at pH_0 1.0 or pH_0 7.0 was left to continue for 24 h as it progressed slowly.

In this paper we have focused on the synthesis of gold nanostructures at pH_0 values of 1.0 (by acidification), 3.4 (without adjustment), and 7.0 (by alkalization).

2.3. Characterization

Transmission electron microscopy (TEM) was carried out on a JEOL JEM-2000EX instrument at an accelerating voltage at 120 kV. High-resolution TEM (HRTEM) was performed on a JEOL JEM-2010 microscope operating at 300 kV. Atomic force microscopy (AFM) measurement was conducted on a Nanoscope IIIa microscope (Digital Instruments, USA) in tapping mode using a silicon nitride tip at room temperature. X-ray diffraction (XRD) was carried out with Rigaku (D/Max-RA) instrument using Cu$K\alpha$ radiation at room temperature. The chemical composition of the products was determined by energy-dispersive X-ray spectroscopy (EDX) using an INCA energy spectrometer (Oxford Instruments, UK). The Fourier transform infrared (FTIR) spectrum was measured on a Nicolet Magna FTIR-750 spectrometer, and UV–vis–NIR spectroscopy was performed on a Shimadzu UV-3150 spectrophotometer.

3. Results and discussion

The formation of nanoparticles starts with nucleation (formation of nuclei as seeds), followed by growth stages [1,21]. Like other face-centered cubic (fcc) metals with intrinsically high symmetry, the most common shape of gold seeds is a spherelike one bounded mainly by {111} and {100} facets due to the lower surface energies of these facets [22]. When the gold precursor is reduced to generate gold atoms at a high enough rate, thermodynamic control will take over in both nucleation and growth: the gold atoms will add homogeneously to all facets of the seeds to form particles with thermodynamically favored shapes, such as cubooctahedrons. However, when the rate of reduction is quite slow, the nucleation and growth of gold are subjected to kinetic control. In the latter case, gold atoms will preferentially add to facets with higher surface energies, which can be promoted by selectively lowering the surface energies of other facets with the help of capping agents [23–25]. As a result, some facets of the seeds will grow more rapidly than other facets, yielding particles with shapes different from those generated under thermodynamic control.

At pH_0 3.4 and 80 °C, the color of the reaction solution changed instantly from light yellow to violet red on addition of aniline, indicating a high rate of reduction that yielded spherical products with an average diameter of 30 nm, as measured by TEM (see Supplementary material). The corresponding selected area electron diffraction (SAED) pattern reveals the characteristic diffractions of fcc gold (see Supplementary material), which is similar to previous reports [19,20]. However, when the pH_0 value was adjusted to about 1.0 after other reaction conditions were fixed, the rate of reduction decreased and the initial light yellow solution changed gradually to colorless, and then purple, followed by a brownish yellow. The obtained gold product consisted of triangular and hexagonal plates about 500 nm to 3 μm in edge size (Fig. 1a). Surface profile analysis of a hexagonal plate by AFM shows that the plate has a thickness of about 45 nm (see Supplementary material). A SAED pattern (Fig. 1b) with hexagonal symmetry diffraction spots was obtained by focusing the electron beams perpendicular to the basal surface of one gold plate lying flat on the TEM grid and indicates that these gold plates are single-crystalline with atomically flat {111} facets as basal surfaces [5,6]. The crystal nature of these gold nanoplates was further studied by XRD. As shown in Fig. 1c, a strong diffraction peak at 38.12° assigned to the {111} lattice facet of fcc gold (Joint Committee on Powder Diffraction Standards File 04-0784) was found, along with much weaker diffractions of other facets, which reflects the highly anisotropic nature of the obtained gold nanoplates and their basal surfaces preferentially orienting parallel to the supporting surface [7,8]. The EDX spectrum recorded from the basal surfaces of these gold nanoplates shows a strong peak arising from gold and two weaker peaks of carbon and nitrogen (see Sup-

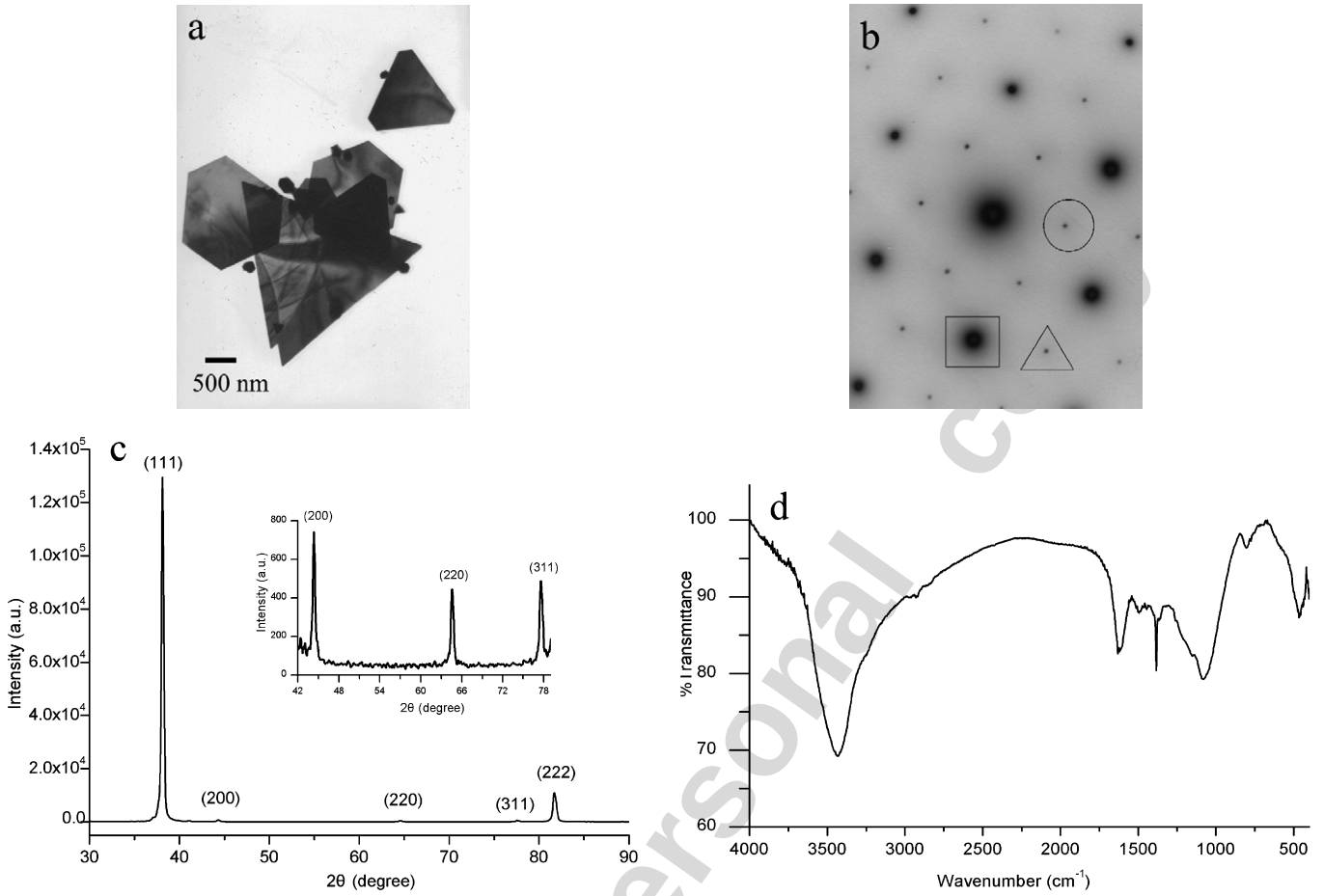

Fig. 1. (a) TEM image of gold nanoplates obtained at pH_0 1.0, 80 °C. (b) The SAED pattern of a single plate; the spots marked using square, triangle, and circle correspond to {220}, {422}, and 1/3{422} diffraction spots of fcc gold. (c) XRD pattern of the as-prepared gold nanoplates. Inset shows the enlarged XRD pattern in the (200), (220), and (311) peak regions. (d) FTIR spectrum of the same batch of gold nanoplates.

plementary material). FTIR spectrum of these gold nanoplates is shown in Fig. 1d. The absorption in the range 3300–3600 cm^{-1} could be assigned to the N–H stretching mode, while the bands located at 1480 and 1595 cm^{-1} are characteristic of the stretching deformation modes of N–B–N (B: benzenoid ring) and N=Q=N (Q: quinoid ring) groups, respectively [26]. These results suggest that these gold nanoplates are covered with the produced polyaniline.

Whereas when the acidity of the $HAuCl_4$ solution was adjusted to lower pH using HCl the color of the solution remained a light yellow, on addition of NaOH to adjust the pH to 7.0 the solution turned nearly colorless, although this change was found to be reversible by lowering the pH again. In the synthesis at pH_0 7.0, the reaction solution quickly turned orange-red and then gradually gray-blue, yielding networked nanowires after further washing of the reaction products with NMP (see Supplementary material). A typical HRTEM image of one part of a wire reveals that the wire consists of prolonged gold particles with a diameter of less than 10 nm (Fig. 2). The SAED pattern (inset of Fig. 2) obtained from the same wire shows the rings corresponding to diffraction from the {111}, {200}, {311}, and {420} facets of fcc gold, which further confirms the polycrystalline nature of these wires.

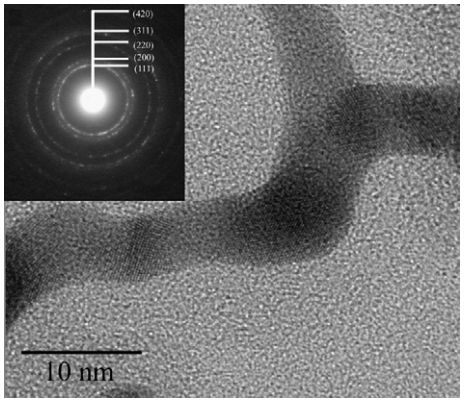

Fig. 2. HRTEM image of a part of nanowire obtained at pH_0 7.0. Inset shows the corresponding SAED pattern.

Why can simply adjusting the pH_0 lead to significant variation in the morphology of the gold nanostructures? As discussed by Gospodinova Terlemezyan in a review article [27], the initial stage of the oxidation polymerization of aniline is the formation of its dimer *N*-phenyl-1,4-benzquinonediimine (C_6H_5–N=C_6H_4=NH, denoted by PBQ), which occurs in the whole pH range. However, the formation rate gets lower in acidic media because the redox potential of aniline increases

with decreasing pH value of the solution. In particular, the formation of PBQ itself is accompanied by a decrease of pH in solution due to the release of H^+, and the reduction of PBQ by aniline during polyaniline formation takes place only at a pH less than 2 [27,28]. Hence, in the synthesis of gold nanoparticles at a pH_0 of 1.0, the rate of reduction of $AuCl_4^-$ turns lower, so that the nucleation and growth of gold becomes subject to kinetic control. Moreover, the polyaniline produced in situ preferentially adsorbs on the {111} facets of the seeds and prevents growth on these facets. As a result, other facets grow more quickly and gold nanoplates bounded mainly by {111} facets are finally generated. In contrast, the reduction proceeds much faster at a pH_0 of 3.4, leading to thermodynamic control over both nucleation and growth and thus yielding spherical gold nanoparticles, regardless of the presence of polyaniline [18,19]. In addition, TEM images of gold nanostructures obtained at other pH_0 values in the range from 1.0 to 3.4 clearly show the shape evolution from plates to spheres with the increase of pH_0, consistent with the above-proposed mechanism (see Supplementary material).

In the synthesis at pH_0 7.0, the color change of $HAuCl_4$ solution upon pH adjustment might be due to the formation of gold hydroxide complexes of the form $[Au(OH)_nCl_{4-n}]^-$. In control experiments, the reaction at pH_0 5.6 proceeded much faster and resulted in short curly nanowires with paramecium-like structures (see Supplementary material). However, no reaction occurred at pH_0 9.0 during the period of 2 h, indicating that the potential of the gold hydroxide complexes might be much lower than that of $AuCl_4^-$. Based on the above data, a possible formation mechanism of the networked wires can be suggested. On addition of aniline at pH_0 7.0, both the high mole ratio of aniline to $AuCl_4^-$ and the decreased redox potential of aniline result in the quick reduction of the remaining $AuCl_4^-$ to gold atoms and then the formation of nuclei. Meanwhile, the gold complex ions are gradually transformed back to $AuCl_4^-$ before being reduced to gold atoms. Subsequently, some nuclei grow into small particles by the conglomeration of the surrounding gold atoms. On the other hand, it would take a relatively long period to reach a pH value less than 2 from the initial neutral solution for further chain propagation of PBQ. Therefore, the small size and the weak capping ability of PBQ and aniline compared with polyaniline bring these nanoparticles into a thermodynamically unstable state. Thus, they would tend to form linear assemblies driven by Brownian motion and short-range interactions, following the deposition of gold atoms on the concave regions of the connected particles through a located Ostwald ripening process [11,29]. Finally, networked gold nanowires are formed.

It is well known that the optical properties of metal nanostructures are strongly related to their shape and size. The UV–vis–NIR absorption spectra of the gold nanostructures obtained at pH_0 values of 1.0, 3.4, and 7.0 exhibit such shape-dependent features, as shown in Fig. 3. For the spherical gold nanoparticles, the spectrum displays a single but strong SPR absorption peak centered at 546 nm (curve a), while the spectrum of the nanoplates shows two broad absorption peaks ranging from 500 to 800 nm and 900 to 1100 nm, respectively, originating from

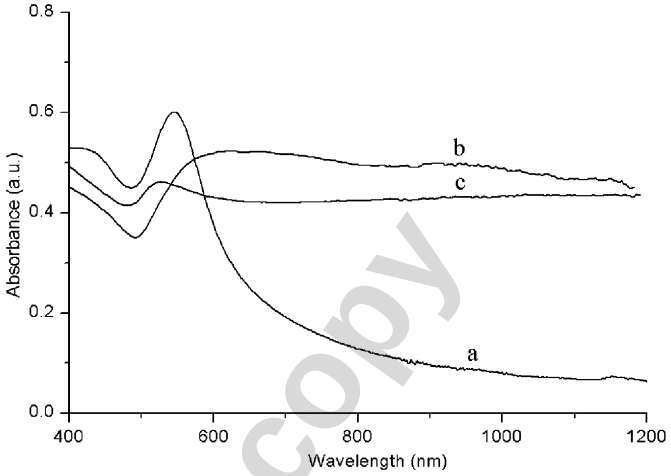

Fig. 3. UV–vis–NIR absorption spectra of the gold nanostructures obtained at 80 °C from solutions at (a) pH_0 3.4, (b) pH_0 1.0, and (c) pH_0 7.0, respectively.

transverse and longitudinal SPR absorption (curve b). The spectrum of the networked gold nanowires (curve c) exhibits a peak at about 520 nm due to the transverse SPR absorption, whereas the flat tail of the spectrum extending into the NIR region can be ascribed to the overlay of the longitudinal SPR absorption of nanowires with different aspect ratios [10,11].

The influence of temperature on the shape of the gold nanostructures was also investigated. Synthesis at 60 °C and pH_0 values of 1.0 and 3.4 yielded larger particles than at the same pH_0 values at 80 °C (Figs. 4a and 4c), which may be explained by the number of gold seeds generated in the nucleation step decreasing at the lower temperature and thus leading to fewer but larger particles [24].

At room temperature, the resulting products at pH_0 1.0 consisted mainly of multilayered structures of gold nanoplates (Fig. 4b). Unlike the random superimposition by dispersed gold nanoplates yielding structures such as those seen in Fig. 4a, these multilayered gold plates in Fig. 4b are inseparable even after extensive ultrasonic treatment of the dilute suspension. The SAED pattern reveals that these gold nanoplates also grow along the {111} facets (see Supplementary material). From a typical TEM image of a partially developed layered structure, it was found that there was a bulge side on the basal surface of the original gold nanoplate, and a new gold nanoplate grew epitaxially from the bulge side, orienting parallel to the original nanoplate (see Supplementary material). Based on these observations, we believe these bulge sides may be ubiquitous on the surfaces of the produced gold nanoplates under the conditions mentioned above and serve as growing flanks of the new nanoplates to form these multilayered structures. Most recently, Yuan et al. also obtained similar structures with preformed sulfonated polyaniline nanotubes as the reductant [30]. However, our method provides a more convenient one-step route to these interesting nanostructures.

In the synthesis at a pH_0 of 3.4, the low reaction rate at room temperature led to the generation of ginger-shaped nanoparticles, as shown in Fig. 4d, with the SAED pattern revealing their polycrystalline nature (see Supplementary material). With respect to the synthesis at a pH_0 of 7.0, however, changing

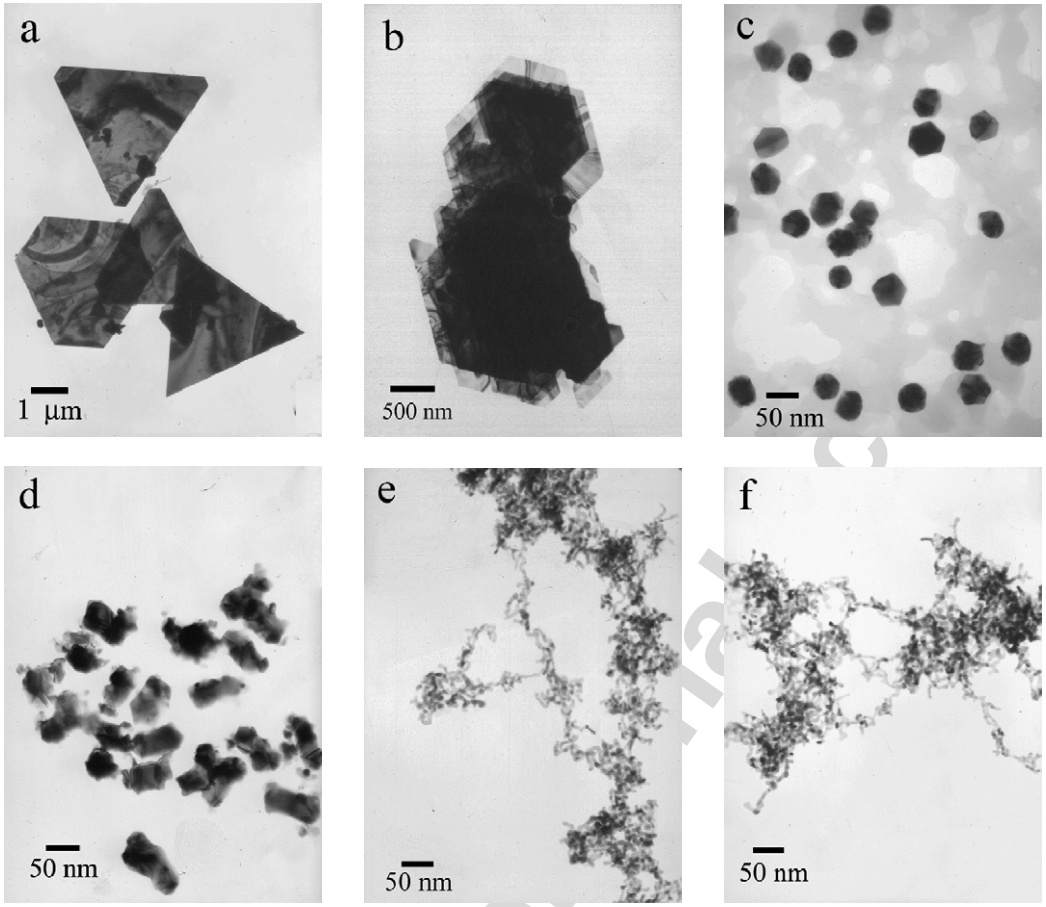

Fig. 4. TEM images of gold nanostructures obtained at a pH_0 of 1.0 and at (a) 60 °C and (b) room temperature, at a pH_0 of 3.4 at (c) 60 °C and (d) room temperature, and at a pH_0 of 7.0 at (e) 60 °C and (f) room temperature.

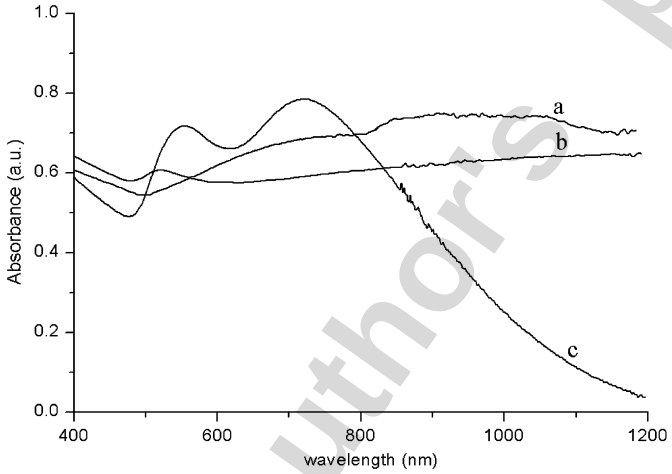

Fig. 5. UV–vis–NIR absorption spectra of gold nanostructures obtained at room temperature, from solutions at (a) pH_0 1.0, (b) pH_0 7.0, and (c) pH_0 3.4, respectively.

the reaction temperature was found to have limited effect on the shape of the gold nanostructures. As shown in Figs. 4e and 4f, the gold nanostructures obtained at decreased temperatures have networked shapes similar to those of the products obtained at 80 °C, something which can be attributed mainly to the weak capping ability of the produced PBQ and aniline, as previously discussed. The UV–vis–NIR spectra of the samples obtained at room temperature are shown in Fig. 5 and their profiles agree well with the corresponding morphologies as observed by TEM.

4. Conclusions

In summary, we have demonstrated a versatile method for preparing anisotropic gold nanostructures including dispersed as well as inseparably multilayered plates, wires with networked or paramecium-like structures, and ginger-shaped particles using aniline as the reductant without the presence of additional stabilizers or capping agents. Control over the particle shapes was achieved by altering the reduction kinetics of $AuCl_4^-$ by varying the pH_0 and the reaction temperature. Moreover, the polyaniline produced in situ serves as an effective capping agent to direct the final shapes by inhibiting the growth of some types of facets of the gold seeds when the growth process is sufficiently slow. These anisotropic gold nanostructures present strongly shape-dependent optical properties as well as intense absorption in the NIR region, which holds potential applications in cancer hyperthermia and IR-absorbing optical coatings [31,32]. In addition, this convenient approach may be applicable to some other anisotropic metal nanostructures such as platinum or palladium.

Acknowledgments

This research was supported by grants (20573019, 60371027, 60171005, and 90406023 from NSFC, China) and the National High-Tech 863 Program. We are thankful to A. Xu and X. Xiao from the Analysis and Testing Center of SEU for their technical assistance. Thanks also to Dr. C.A. Ohlin for help with preparation of the manuscript.

Supplementary material

The online version of this article contains additional supplementary material.

Please visit DOI: 10.1016/j.jcis.2006.12.070.

References

[1] H. Bönnemann, R.M. Richards, Eur. J. Inorg. Chem. (2001) 2455.
[2] M.-C. Daniel, D. Astruc, Chem. Rev. 104 (2004) 293.
[3] J. Gao, C.M. Bender, C.J. Murphy, Langmuir 19 (2003) 9065.
[4] I. Balint, A. Miyazaki, K.A. Aika, Appl. Catal. B 37 (2002) 217.
[5] S.S. Shankar, A. Rai, B. Ankamwar, A. Singh, A. Ahmad, M. Sastry, Nat. Mater. 3 (2004) 482.
[6] L. Wang, X. Chen, J. Zhan, Y. Chai, C. Yang, L. Xu, W. Zhuang, B. Jing, J. Phys. Chem. B 109 (2005) 3189.
[7] Z. Li, Z. Liu, J. Zhang, B. Han, J. Du, Y. Gao, T. Jiang, J. Phys. Chem. B 109 (2005) 14445.
[8] C. Li, W. Cai, B. Cao, F. Sun, Y. Li, C. Kan, L. Zhang, Adv. Funct. Mater. 16 (2006) 83.
[9] J. Sharma, K.P. Vijayamohanan, J. Colloid Interface Sci. 298 (2006) 679.
[10] C. Chen, Y. Yeh, C.R.C. Wang, J. Phys. Chem. Solids 62 (2001) 1587.
[11] L. Pei, K. Mori, M. Adachi, Langmuir 20 (2004) 7837.
[12] S. Gao, H. Zhang, X. Liu, X. Wang, L. Ge, J. Colloid Interface Sci. 293 (2006) 409.
[13] A. Swami, A. Kumar, P.R. Selvakannan, S. Mandal, R. Pasricha, M. Sastry, Chem. Mater. 15 (2003) 17.
[14] O.M. Bakr, B.H. Wunsch, F. Stellacci, Chem. Mater. 18 (2006) 3297.
[15] E. Hao, R.C. Bailey, G.C. Schatz, J.T. Hupp, S. Li, Nano Lett. 4 (2004) 327.
[16] X. Zheng, L. Zhu, X. Wang, A. Yan, Y. Xie, J. Cryst. Growth 260 (2004) 255.
[17] J. Hu, Y. Zhang, B. Liu, J. Liu, H. Zhou, Y. Xu, Y. Jiang, Z. Yang, Z. Tian, J. Am. Chem. Soc. 126 (2004) 9470.
[18] H. Nakao, H. Shiigi, Y. Yamamoto, S. Tokonami, T. Nagaoka, S. Sugiyama, T. Ohtani, Nano Lett. 3 (2003) 1391.
[19] C. Subramaniam, R.T. Tom, T. Pradeep, J. Nanopart. Res. 7 (2005) 209.
[20] G. Zheng, Y. Shao, B. Xu, Acta Chim. Sinica 64 (2006) 733.
[21] B.L. Cushing, V.L. Kolesnichenko, C.J. O'Connor, Chem. Rev. 104 (2004) 3893.
[22] B. Wiley, Y. Sun, J. Chen, H. Cang, Z. Li, X. Li, Y. Xia, MRS Bull. 30 (2005) 366.
[23] L. Lu, A. Kobayashi, K. Tawa, Y. Ozak, Chem. Mater. 18 (2006) 4894.
[24] Y. Xiong, J.M. McLellan, J. Chen, Y. Yin, Z. Li, Y. Xia, J. Am. Chem. Soc. 127 (2005) 17118.
[25] C. Lofton, W. Sigmund, Adv. Funct. Mater. 15 (2005) 1197.
[26] T.K. Sarma, D. Chowdhury, A. Paul, A. Chattopadhyay, Chem. Commun. (2002) 1048.
[27] N. Gospodinova, L. Terlemezyan, Prog. Polym. Sci. 23 (1998) 1443.
[28] N. Gospodinova, P. Mokreva, L. Terlemezyan, Polymer 34 (1993) 2438.
[29] C. Huang, Y. Wang, P. Chiu, J. Lin, Chem. Lett. 35 (2006) 30.
[30] J. Yuan, Z. Wang, Q. Zhang, D. Han, Y. Zhang, Y. Shen, L. Niu, Nanotechnology 17 (2006) 2641.
[31] L.R. Hirsch, R.J. Stafford, J.A. Bankson, S.R. Sershen, B. Rivera, R.E. Price, J.D. Hazle, N.J. Halas, Proc. Natl. Acad. Sci. USA 100 (2003) 13549.
[32] S.S. Shankar, A. Rai, A. Ahmad, M. Sastry, Chem. Mater. 17 (2005) 566.